Journal of Alloys and Compounds 556 (2013) 1–5

Contents lists available at SciVerse ScienceDirect

Journal of Alloys and Compounds

journal homepage: www.elsevier.com/locate/jalcom

Blue-shift of UV emission in ZnO/graphene composites

Jinghai Yang [a,b,*], Xiaoting Zhao [a,b], Xiaonan Shan [c], Hougang Fan [a,b], Lili Yang [a,b], Yongjun Zhang [a,b], Xiuyan Li [a,b]

[a] Institute of Condensed State Physics, Jilin Normal University, Siping 136000, People's Republic of China
[b] Key Laboratory of Functional Materials Physics and Chemistry, Jilin Normal University, Ministry of Education, Siping 136000, People's Republic of China
[c] Key Laboratory of Excited State Physics, Changchun Institute of Optics Fine Mechanics and Physics, Chinese Academy of Sciences, Changchun 130033, People's Republic of China

ARTICLE INFO

Article history:
Received 28 June 2012
Received in revised form 26 November 2012
Accepted 20 December 2012
Available online 29 December 2012

Keywords:
ZnO
Graphene
Blue shift
Burstein–Moss effect
PL quenching

ABSTRACT

ZnO and graphene composites (ZnO/GR) were prepared by a simple and repeatable thermal evaporation process, and both the reduction of graphene oxide and the loading of ZnO were achieved. The structural and optical properties were studied by X-ray diffraction (XRD), scanning electron microscopy (SEM), transmission electron microscope (TEM), atomic force microscope (AFM), Raman spectroscopy, X-ray photoelectron spectroscopy (XPS) and photoluminescence (PL) measurements. In the PL spectra, when the mass ratio of graphene to ZnO increased, a series of fluorescence quenching were found, and a regularly blue shift of the ultraviolet (UV) peak were also found, which might be attributed to the Burstein–Moss effect.

1. Introduction

The two-dimensional (2D) graphene exhibited a promising potential in fabricating electronic devices due to its fascinating physical properties such as quantum electronic transport, extremely high mobility, high elasticity and electromechanical modulation [1–4]. One way to utilize the unique properties of graphene would be its incorporation in a composition. Recently, the graphene sheets decorated by the inorganic nanoparticles (NPs) such as metal, metal oxide and sulfide, i.e. the graphene/inorganic composites, have attracted uncountable attention. So far, some graphene/inorganic composites have been successfully synthesized and showed the desirable properties that cannot be found in the individual component [5–15]. As an important wide band-gap semiconductor, ZnO has already been evaluated in the application of optoelectronic devices such as solar cells, gas sensors and light emitting diodes, due to its promising electrical and optical properties [16–18]. The new ZnO/GR composites might possess unusual properties as compared with their individual counterpart, and present some special features, such as high electrical property, good optical transmittance, improved field emission and capacitive properties, which prompt many researchers to synthesize the ZnO/GR composites and explore their potential applications [19–21].

For most chemistry methods, the graphene oxide is usually reduced into graphene with toxic reductant [22], such as hydrazine. The worse thing is that the reduction process could lead to more defects in graphene and the graphene would restack together to form graphite [23]. Recently the non-toxic water had been reported to reduce graphene oxide under specific condition [24], which had fewer defects in graphene and no restacking of graphene.

In this work, we have prepared ZnO/GR composites by an easy and reproducible one-step thermal evaporation reaction. In the solvent of water, ZnO particles can attach on the surface and edge of graphene oxide sheets, which could efficiently separate the graphene sheets and prevent the restacking of the graphene sheets. Therefore the ZnO/GR composites can be directly formed during the reduction of the graphene oxide. We have studied the structural and optical properties of ZnO/GR composites with different ratios.

2. Experimental

2.1. Preparation of graphene oxide

Graphene oxide (GO) was prepared by a modified Hummers method [25,26] from flake graphite (average particle diameter of 25 mm, 99.9% purity, Qingdao Weijie Graphite Co., Ltd.). Briefly, 1 g of graphite and 1 g of $NaNO_3$ were placed in a beaker. The 50 mL of H_2SO_4 was added into the beaker. The mixture was stirring at 80 °C for 1 h. Then, 6 g of $KMnO_4$ powder was slowly added over 1 h in an ice water bath. Cooling was completed in 2 h, and the mixture was allowed to vigorous stirring 3 h at room temperature. During which the mixture turns green, dark brown, and then brick brown. The obtained liquid was added with 300 mL de-ionized water and then stirred over about 30 min at 98 °C. When the temperature was

* Corresponding author at: Institute of Condensed State Physics, Jilin Normal University, Siping 136000, People's Republic of China. Tel.: +86 434 329456.
E-mail address: jhyang1@jlnu.edu.cn (J. Yang).

0925-8388/$ - see front matter © 2012 Elsevier B.V. All rights reserved.
http://dx.doi.org/10.1016/j.jallcom.2012.12.098

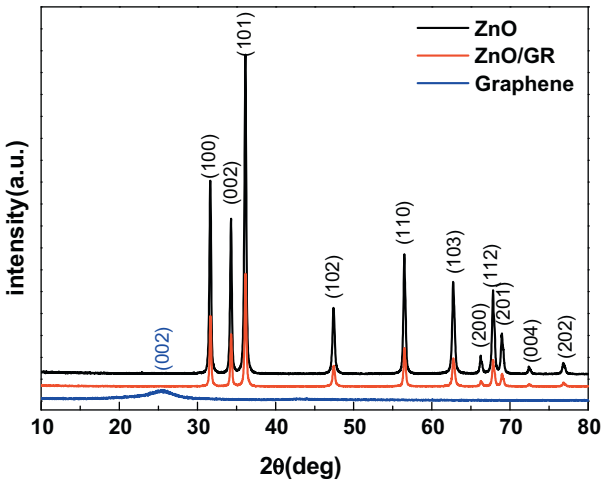

Fig. 1. XRD pattern of the prepared ZnO, ZnO/GR, and graphene.

cooled down to 60 °C 30 mL of H_2O_2 (30 wt.% aqueous solution) was added into the above liquid. In order to remove ions of oxidant, the resultant liquid was purified by repeating the following procedure cycle 3 times: centrifugation, removal of the supernatant liquid, adding some 5% HCl with vigorous stirring and bath ultrasonication for 30 min at a power of 100 W. Then the procedure was cycled for 3 times using de-ionized water. The remainder was dried at 60 °C for 24 h, and then the graphene oxide was obtained.

2.2. Preparation of ZnO/GR

The graphene oxide powder obtained above (1 mg/mL) was added into ZnO colloidal suspension (40 mg/mL commercial ZnO nanoparticles with particle diameter of 10 nm (Hurricane Co., Iran) in water). The suspension was vigorously stirred for 2 h, sonicated for 30 min and subsequently heated at 200 °C to obtain the hybridized ZnO/GR powder.

X-ray diffraction (XRD) was performed on a Rigaku-Dmax-Ra powder X-ray diffractometer with Cu Kα radiation (λ = 1.5418 A). The morphology of the samples was carried out through scanning electron microscopy (SEM) (Hitachi, S-570) and Transmission electron microscope (TEM) (200 keV, JEM-2010HR). To characterize the surface topography of the graphene sheets, Atomic Force Microscope (AFM) (Bruker-Veeco Multimode Nanoscope 3d) was utilized as an appropriate technique. The chemical components were characterized by X-ray photoelectron spectroscopy (XPS) (ESCALABMKLL). The Raman and photoluminescence (PL) spectra were performed on the Renishaw invia Raman spectroscopy. The excitation wavelength for Raman measurement is 514.5 nm originated from Ar^+ Laser. The excitation source for PL measurement was He–Cd Laser with 325 nm wavelength.

3. Results and discussion

Fig. 1 showed that the typical diffraction peak of GO at 2 h = 10.6° [27] shifts to higher angle after reduction. This could be attributed to fact that GO nanosheets are partially reduced to graphene and restacked into an ordered crystalline structure. The XRD pattern of ZnO/GR composites with 1 mM ZnO suspension and 0.025 mg/mL at GR concentrations was similar to that of pure ZnO. And no diffraction peaks for carbon species were found, which might be owing to the low amount and relatively low diffraction intensity of graphene.

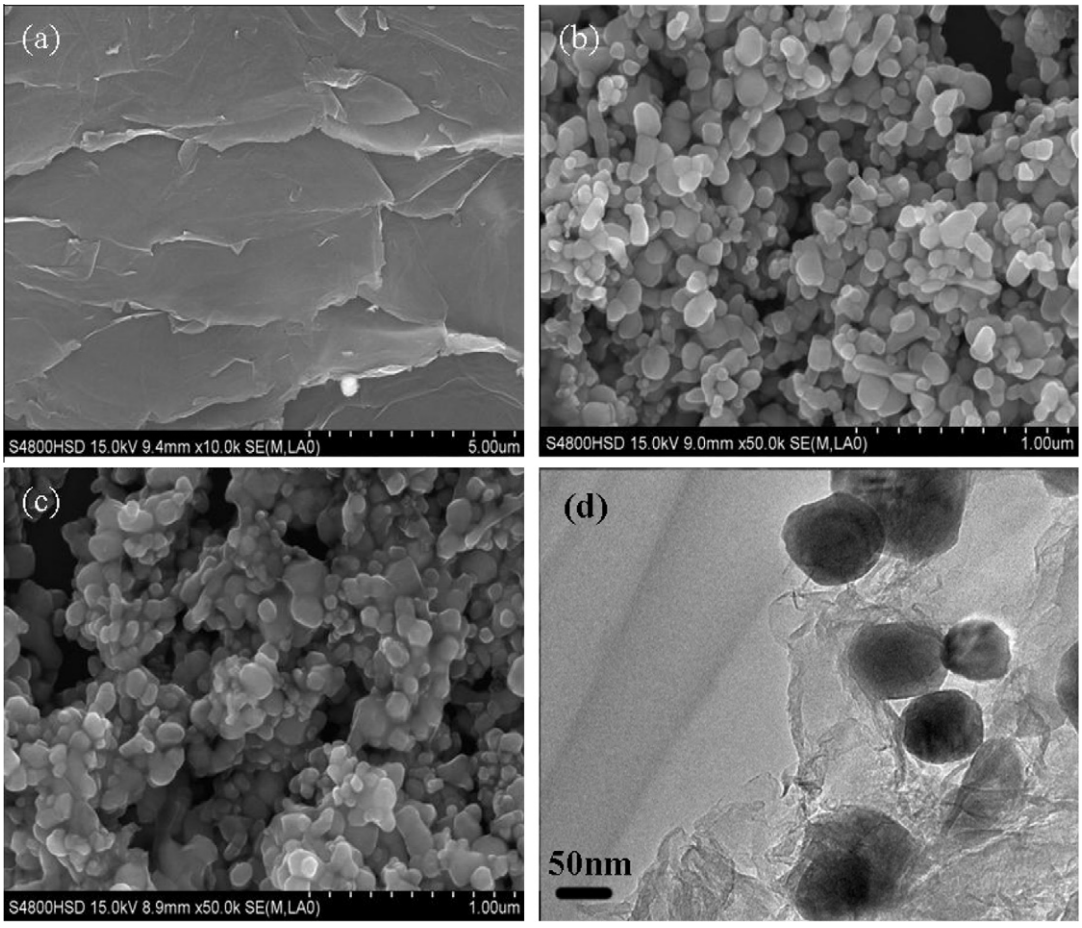

Fig. 2. FESEM of (a) GO, (b) ZnO, (c) ZnO/GR and TEM of (d) ZnO/GR.

Fig. 2a showed the SEM images of GO with lots of wrinkles which were probably caused by the oxygen functionalization and the resultant defects during the preparation. Fig. 2b and c showed the SEM images of ZnO and the ZnO/GR composites with 1 mM ZnO suspension at GR concentration 0.025 mg/mL, which revealed graphene sheets emerged and the ZnO nanoparticles were dispersed and coated by graphene sheets. The formation graphene sheet decorated by ZnO nanoparticles was further investigated by TEM with 1 mM ZnO suspension at different GR concentrations 1 mg/mL in Fig. 2d. The 2D graphene sheets and ZnO nanoparticles were clearly observed. The graphene sheets were not perfectly flat but display intrinsic microscopic roughening and out of plane deformations (wrinkles).

A typical AFM image of ZnO nanoparticles anchored to graphene sheets was given in Fig. 3, which were consistent with the TEM image. The corresponding section-depth profile of the image is also provided. The height profile diagram of the AFM image showed that the height of the graphene layer was about 1.35 nm, which is in good consistency with the typical thickness of the observed bilayer graphene based on theoretical values of 0.78 nm for single layer graphene and the thickness contribution form oxygen-containing groups on the faces [28].

In the XPS spectra (Fig. 4a), the level of $Zn_{2p}{}^{3/2}$ is 1020.39 eV. The peaks located at 284.6 and 530.4 eV are assigned to the peaks of C_{1s} and O_{1s}, respectively. The peaks at 288.7 eV in the C_{1s} spectra are assigned to the carbon element in association with oxygen in the carbonate ions. The predominant O_{1s} peak at 530.4 eV belongs to the lattice oxygen of the ZnO NPs. The remaining smaller peaks at higher binding energies (760.7, 795.4, 816.7 eV) are satellite shake-ups of the assigned components [29]. Fig. 4b showed that the concentration of the oxygen–containing bonds(C—OH, C═O and O═C—OH in the reduced graphene sheets) were very low, which indicated an effective chemical reduction of the graphene oxide platelets to graphene ones in the ZnO/graphene (oxide) suspension. Thermal evaporation is a convenient method to convert GO sheets to graphene sheets. The high temperature made GO reduced to graphene [24].

Raman spectroscopy was used to characterize the ordered disordered crystal structures of carbon materials [30]. As shown in Fig. 5, Raman spectra of ZnO/GR composites showed two fundamental vibrations. *G* band located at 1580 cm^{-1} which is generally assigned to the E_{2g} phonon of sp^2 bonds of carbon atoms. *D* band located at 1357 cm^{-1} as a breathing mode of π-point phonons of A_{1g} symmetry [31,32], which is attributed to local defects and disorders, particularly the defects located at the edges of graphene and graphite platelets [33,34]. The fitting of the observed Raman spectra using the Raman spectrometer software gives the D/G intensity ratios which listed in Table 1. One can see there is no regular evolution for the D/G intensity ratios evolution with the increasing of the GR concentrations from 0.025 mg/mL to 5 mg/mL. The D/G intensity ratio for all ZnO/GRs is around 0.90, which are larger than that of GO (0.75). This suggests that more sp^2 domains are formed during the reduction of GO, and indicates that there is increasing disorder in ZnO/GR. The peak at 2937 cm^{-1} associating with the D + G band also indicates the increasing disorder in graphene [33,34].

The optical property was characterized by the room-temperature PL spectroscopy. As shown in Fig. 6, the PL spectra of ZnO and ZnO/GR composites showed the dominant UV emission at 386 nm which was attributed to free-excitation recombination in the near-band-edge. From curves *a* to *d*, the UV emission peak position gradually shifted from 384 to 379 nm (Fig. 7). While the PL intensity decreased gradually. We believe that the blue-shift of the UV emission peak originated from the interaction between the ZnO particles and the graphene sheets. The physical mechanism might be attributed to the Burstein–Moss effect [35,36]. As shown in Fig. 8, the calculated work function for graphene is 4.4 eV [37,38], which is lower than that for ZnO (4.5 eV) [39]. When ZnO/GR composites formed, some electrons of graphene sheets may diffuse towards the ZnO and accumulate at the interface between the graphene and ZnO to form potential barrier. The barriers impede the diffusion of the electron into ZnO. Those electrons may occupy the states at the bottom of the conduction band of ZnO. After the thermal relaxation, there is a considerable population in the low energy levels of the conduction band. Thus the photo excitation electrons of ZnO requires $E_g + \Delta E_b$ energy, where ΔE_b is the extra energy required to transfer the free electrons to the unoccupied electronic sublevels closest to the bottom of the conduction band. This shift in ΔE_b is called the Burstein Moss shift. With increase of the mass ratio of graphene to ZnO, more π electrons would enter the lattice of ZnO. The potential barrier formed between the graphene and ZnO would increase. Thus the Burstein Moss shift ΔE_b would be increased also. As a result, the optical band-gap became larger gradually. As the optical band-gap increased, the number of the photogenerated electrons in ZnO would also decrease gradually, which would make the PL intensity decreasing.

The weak deep level emission appeared in the PL curve located at around 550–590 nm. The ability of ZnO particles to transfer photogenerated electrons to GO has been demonstrated from the quenching of ZnO emission [40]. The fluorescence intensity decreased as the amount of GO increasing. The interaction between the excited ZnO particles and the GO sheets results in an additional

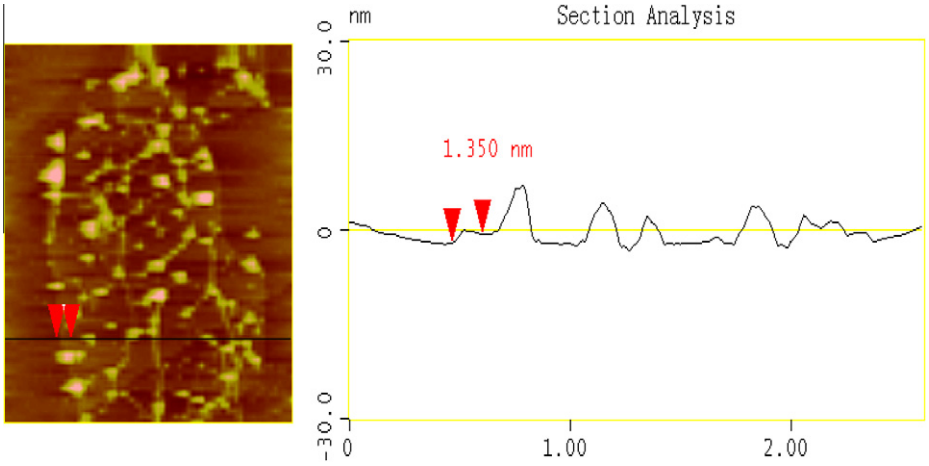

Fig. 3. AFM images of the ZnO/GR with 1 mM ZnO suspension at GR concentrations 1 mg/mL on mica substrates.

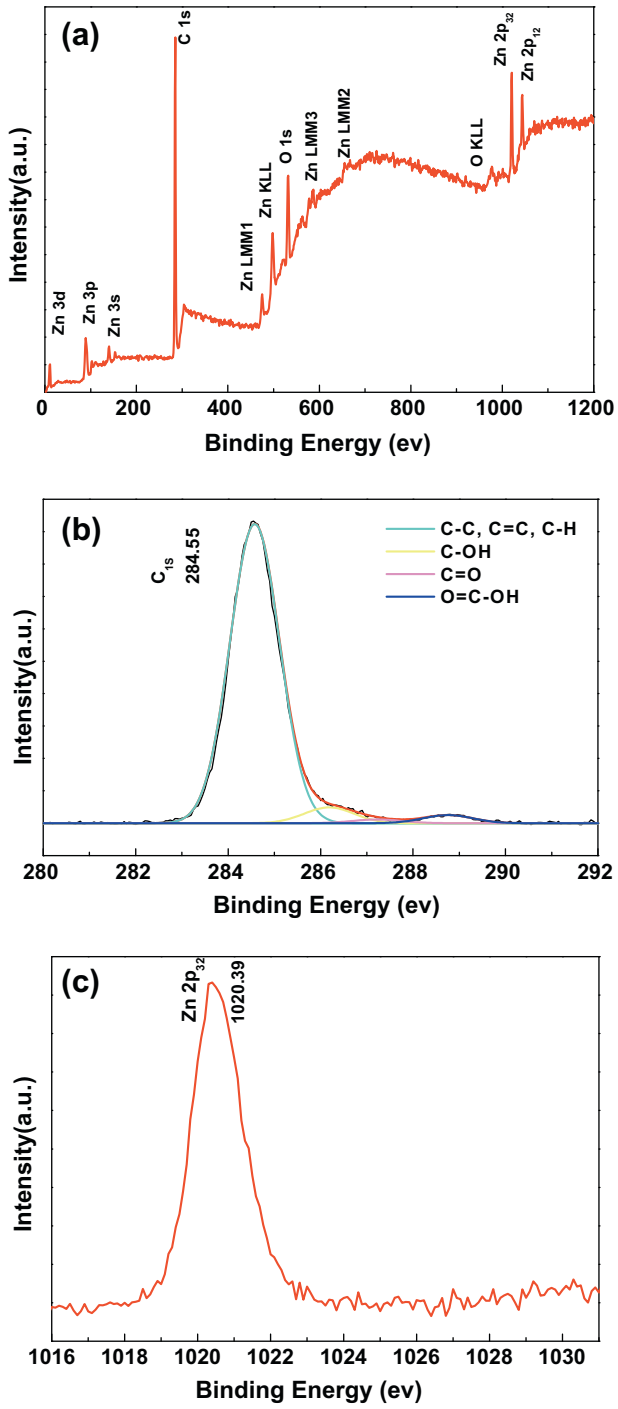

Fig. 4. The XPS spectra of the ZnO/GR with 1 mM ZnO suspension at GR concentrations 0.025 mg/mL.

pathway for the disappearance of the charge carriers. As demonstrated earlier, such emission quenching represents interfacial charge-transfer processes [41–43]. In the present experiments, the emission quenching represented electron transfer from the

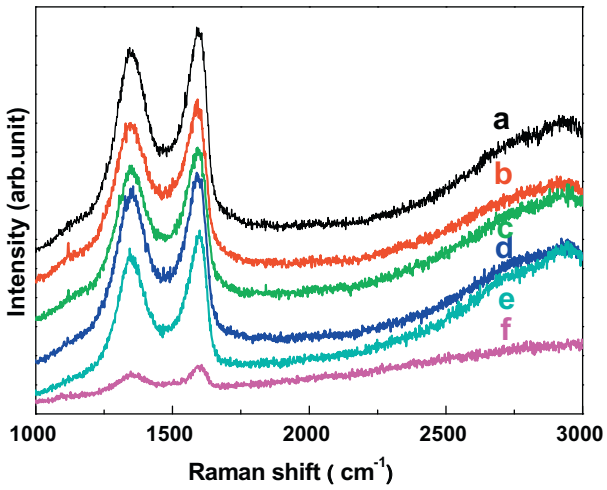

Fig. 5. Raman spectra of graphene and ZnO/GR composites. Samples *a* to *f* represent 1 mM ZnO suspension at different GR concentrations: (a) 0.025, (b) 0.033, (c) 0.05, (d) 0.1, (e) 1, and (f) 5 mg/mL.

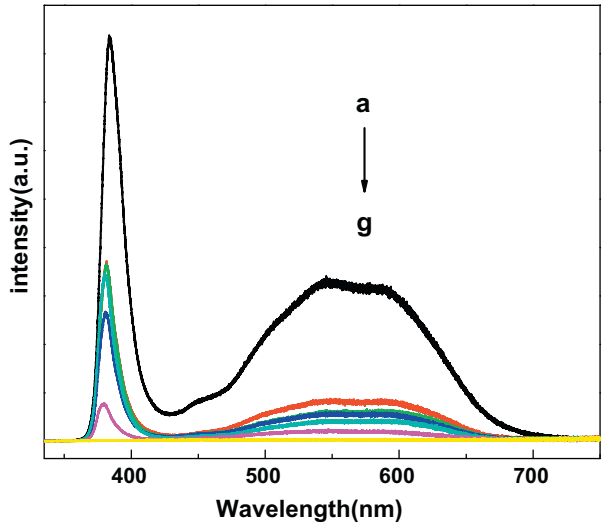

Fig. 6. Room temperature PL spectra of a–g represent 1 mM ZnO suspension at different GR concentrations: (a) 0, (b) 0.025, (c) 0.033, (d) 0.05, (e) 0.1, (f) 1, and (g) 5 mg/mL.

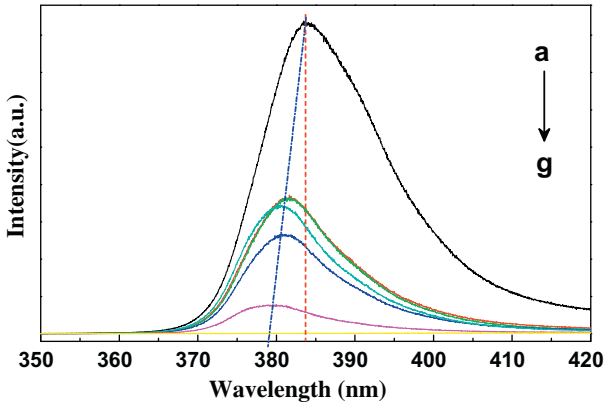

Fig. 7. The blue shift of the UV peak. (For interpretation of the references to colour in this figure legend, the reader is referred to the web version of this article.)

Table 1
The D/G intensity ratios of Raman spectra for all samples.

Sample	*a*	*b*	*c*	*d*	*e*	*f*
D/G ratio	0.92	0.89	0.90	0.89	0.93	0.91

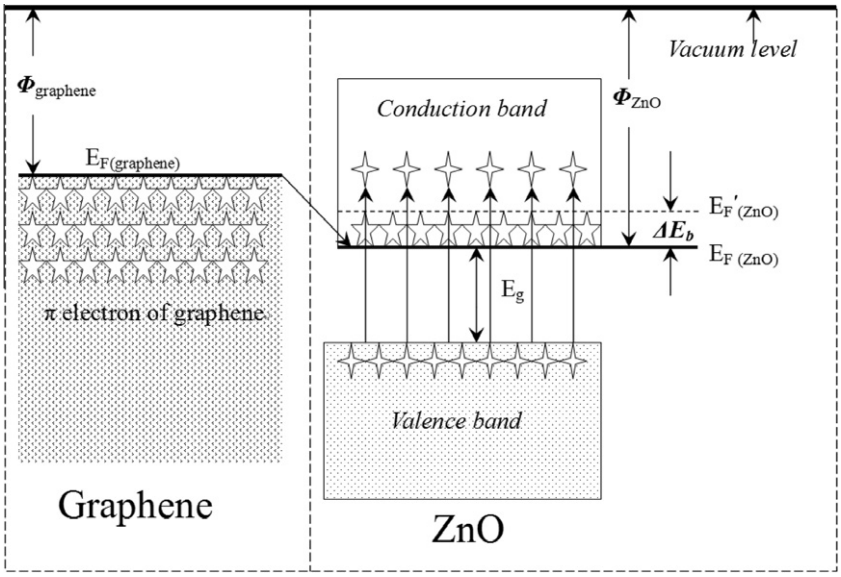

Fig. 8. Schematic of the Burstein–Moss shift in ZnO/GR.

excited ZnO NPs to the GO to produce reduced graphene. Without ZnO, no such reductive radicals are produced. The charge recombination in semiconductor particulates is often a problem in heterogeneous photocatalysis by semiconductor materials (TiO_2, ZnO, ZnS, etc.) [5–11]. If semiconductor particles are anchored on a graphene scaffold, it should be possible to improve the photo induced charge separation and then improve the photocatalysis performance.

4. Conclusion

In summary, we demonstrated a repeatable route to obtain ZnO/GR composites by a thermal evaporation reaction. The blue-shift of UV emission peaks in the PL spectra of ZnO/GR composites might be attributed to the Burstein–Moss effect. The PL quenched phenomenon implied that the recombination of the photo induced charge would be restrained, which will benefit the heterogeneous photocatalysis of semiconductor materials. This work opens up new avenues to one-step synthesis of graphite-based composites in various solvents, i.e. the nanomaterial synthesis and reduction of GO sheets to graphene sheets could occur simultaneously.

Acknowledgments

This work is supported by the National Natural Science Foundation of China (Grant Nos. 61178074 and 61008051), Program for the Development of Science and Technology of Jilin Province (Item Nos. 201105084 and 201115219), the Twentieth Five-Year Program for Science and Technology of Education Department of Jilin Province (Item No. 20110170), Program for the master students' scientific and innovative research of Jilin Normal University (Item Nos. 201139 and 201141).

References

[1] K.S. Novoselov, A.K. Geim, S.V. Morozov, D. Jiang, M.I. Katsnelson, I.V. Grigorieva, S.V. Dubonos, A.A. Firsov, Nature 438 (2005) 197.
[2] A.K. Geim, K.S. Novoselov, Nat. Mater. 6 (2007) 183.
[3] K.S. Novoselov, Z. Jiang, Y. Zhang, S.V. Morozov, H.L. Stormer, U. Zeitler, J.C. Maan, G.S. Boebinger, P. Kim, A.K. Geim, Science 315 (2007) 1379.
[4] D. Li, R.B. Kaner, Science 320 (2008) 1170.
[5] P. Zeng, Q.G. Zhang, X.G. Zhang, T.Y. Peng, J. Alloys Comp. 516 (2012) 85.
[6] X.D. Huang, X.F. Zhou, K. Qian, D.Y. Zhao, Z.P. Liu, C.Z. Yu, J. Alloys Comp. 514 (2012) 76.
[7] D.F. Qian, Y.G. Li, Q.H. Zhang, J. Alloys Comp. 509 (2011) 10121.
[8] T. Lv, L.K. Pan, X.J. Liu, T. Lu, G. Zhu, Z. Sun, J. Alloys Comp. 509 (2011) 10086.
[9] G. Wang, T. Liu, Y.J. Luo, Y. Zhao, Z.Y. Ren, J.B. Bai, H. Wang, J. Alloys Comp. 509 (2011) L216.
[10] X.P. Shen, J.L. Wu, S. Bai, H. Zhou, J. Alloys Comp. 506 (2010) 136.
[11] T. Lu, L.K. Pan, H.B. Li, G. Zhu, T. Lv, X.J. Liu, Z. Sun, T. Chen, Daniel H.C. Chua, J. Alloys Comp. 509 (2010) 5488.
[12] G. Williams, P.V. Kamat, Langmuir 25 (24) (2009) 13869.
[13] D.H. Wang, D.W. Choi, J. Li, Z.G. Yang, Z.M. Nie, R. Kou, D.H. Hu, C.M. Wang, L.V. Saraf, J.G. Zhang, I.A. Aksay, J. Liu, ACS Nano 3 (2009) 907.
[14] S.M. Paek, E. Yoo, I. Honma, Nano Lett. 9 (2009) 72.
[15] G. Williams, B. Seger, P.V. Kamat, ACS Nano 2 (2008) 1487.
[16] J. Li, H. Fan, X. Jia, J. Chen, Z. Cao, X. Chen, J. Alloys Comp. 481 (2009) 735.
[17] W. Yan, H. Fan, C. Yang, Mat. Lett. 65 (2011) 1595.
[18] H. Gómez, A. Maldonado, R. Castanedo-Pérez, G. Torres-Delgado, M.delaL. Olvera, Mater. Charact. 58 (2007) 708.
[19] J.M. Lee, Y.B. Pyun, J. Yi, J.W. Choung, W.I. Park, J. Phys. Chem. C 113 (2009) 19134.
[20] W.T. Zheng, Y.M. Ho, H.W. Tian, M. Wen, J.L. Qi, Y.A. Li, J. Phys. Chem. C 113 (2009) 9164.
[21] Y. Zhang, H. Li, L. Pan, T. Lu, Z. Sun, J. Electroanal. Chem. 634 (2009) 68.
[22] T.N. Zhou, F. Chen, C.Y. Tang, H.W. Bai, Q. Zhang, H. Deng, Q. Fu, Compos. Sci. Technol. 71 (2011) 1266.
[23] K. Behfar, R. Naghdabadi, Compos. Sci. Technol. 65 (2005) 1159.
[24] C. Nethravathi, R. Michael, Carbon 46 (2008) 1994.
[25] W.S. Hummers, R.E. Offeman, J. Am. Chem. Soc. 80 (1958) 1339.
[26] Y. Wang, Y.M. Li, L.H. Tang, J. Lu, J.H. Li, Electrochem. Commun. 11 (2009) 889.
[27] H.K. Jeong, Y.P. Lee, R. Lahaye, M.H. Park, K.H. An, I.J. Kim, et al., J. Am. Chem. Soc. 130 (2008) 1362.
[28] H.B. Li, T. Lu, L.K. Pan, Y.P. Zhang, Z. Sun, J. Mater. Chem. 19 (2009) 6773.
[29] C.E. Hamilton, J.R. Lomeda, Z.Z. Sun, J.M. Tour, A.R. Barron, Nano Lett. 9 (2009) 3460.
[30] D. Graf, F. Molitor, K. Ensslin, C. Stampfer, A. Jungen, C. Hierold, et al., Nano Lett. 7 (2007) 238.
[31] F. Tuinstra, J.L. Koenig, J. Chem. Phys. 53 (1970) 1126.
[32] A.C. Ferrari, J. Robertson, Phys. Rev. B 61 (2000) 14095.
[33] C. Ferrari, J.C. Meyer, V. Scardaci, C. Casiraghi, M. Lazzeri, F. Mauri, S. Piscanec, D. Jiang, K.S. Novoselov, S. Roth, A.K. Geim, Phys. Rev. Lett. 97 (2006) 187401.
[34] Z.H. Ni, H.M. Wang, J. Kasim, H.M. Fan, T. Yu, Y.H. Wu, Y.P. Feng, Z.X. Shen, Nano Lett. 7 (2007) 2758.
[35] E. Burstein, Phys. Rev. 93 (1954) 632.
[36] T.S. Moss, Proc. Phys. Soc. London B76 (1954) 775.
[37] Z.F. Liu, Q. Liu, Y. Huang, Y.F. Ma, S.G. Yin, X.Y. Zhang, W. Sun, Y.S. Chen, Adv. Mater. 20 (2008) 3924.
[38] R. Czerw, B. Foley, D. Tekleab, A. Rubio, P.M. Ajayan, D.L. Carroll, Phys. Rev. B 66 (2002) 033408.
[39] K.B. Sundaram, A. Khan, J. Vac. Sci. Technol. A 15 (1997) 428.
[40] F. Vietmeyer, B. Seger, P.V. Kamat, Adv. Mater. 19 (2007) 2935.
[41] P.V. Kamat, B. Patrick, J. Phys. Chem. 96 (1992) 6829.
[42] V. Subramanian, E.E. Wolf, P.V. Kamat, J. Phys. Chem. B 107 (2003) 7479.
[43] P.V. Kamat, R. Huehn, R. Nicolaescu, J. Phys. Chem. B 106 (2002) 788.